Skin strain fields at the shoulder joint for mechanical counter pressure space suit development

Edward W. Obropta
Massachusetts Institute of Technology
77 Massachusetts Ave. Cambridge, MA 02139
617-253-5487
eobropta@mit.edu

Dava J. Newman
Massachusetts Institute of Technology
77 Massachusetts Ave. Cambridge, MA 02139
617-258-8799
dnewman@mit.edu

***Abstract*—High-resolution human skin strain field data is presented for the shoulder joint measured using three-dimensional digital image correlation (3D-DIC). Developing mechanical counter pressure (MCP) space suits requires detailed understanding of human skin deformation at joints in order to fit and create MCP without restricting human mobility or increasing human energy expenditure. Previously, skin strain for this application has been measured for one degree of freedom joints such as the elbow and knee. Now using four stereoscopic camera pairs for 3D-DIC (8 cameras), a strain field comparison is made between various motions of the shoulder joint. This paper specifically compares shoulder abduction and flexion in the context of realizing a MCP space suit designed for planetary exploration. Methods are explained to perform 3D-DIC using multiple stereoscopic camera pairs for complex joint motions. These results are important to develop MCP space suits that allow upper-body mobility. The discussion of the results provides insight and data for designing optimal textile patterning for skin-tight space suits at multiple-degree of freedom joints.**

TABLE OF CONTENTS

1. INTRODUCTION

In order to experience space first hand, we need space suits to protect us from the extreme environment. The current space suits are problematic for planetary exploration because they limit astronaut mobility and cause exhaustion [1]. In the mid-1900s, Arthur Iberall researched how to design mobile pressurized space suits. He used information from the deformation of human skin to develop the concept of the Lines of Non-extension (LoNEs). He describes these LoNEs as contours along the human body where the skin does not stretch [2]. Annis and Webb also developed approaches to make mobile space suits. They developed the Space Activity Suit, a mechanical counter pressure (MCP) space suit that used material elasticity to pressurize the body instead of gas pressure [3]. They tested this concept in 1971, but concluded that the ideal materials did not exist and the suit was too difficult to don and doff. At the time, the gas pressurized suits were more technologically feasible. In 2001, the concept of a fully MCP spacesuit reemerged at the Massachusetts Institute of Technology (MIT) as the BioSuit™, which was inspired by Iberall, Annis, and Webb [4,5]. The BioSuit™ is designed to be like a second-skin garment. The concepts of MCP have also been applied to different components of space suits, such as gloves that have been tested by Clapp, Tanaka *et al.*, and Waldie *et al.*, which have been shown to provide increased mobility [6–8].

The energy required to arbitrarily deform a space suit can be expressed as:

$$\Delta W = \Delta W_p + \Delta W_b + \Delta W_s, \tag{1}$$

where the work required to change the gas pressure and volume of the suit is ΔW_p, the work to bend the suit's material is ΔW_b, and the work required to stretch the suit's material is ΔW_s [2]. In gas pressurized suits, significant effort is placed on minimizing the pressure-volume effects [9]. However, many soft gas pressurized suits remain difficult to move and bend primarily because of work contributed by ΔW_p [10]. Hard suits often utilize rotating bearings to maintain constant internal volume, but tend to be cumbersome and result in unnatural human motion. Contrarily, MCP suits do not contain pressurized gas and therefore do not have the W_p term. This makes the work to deform MCP suits dependent on the mechanical deformation expressed in $\Delta W_b + \Delta W_s$ [11], which is the tradeoff of MCP designs. If the material is designed to deform similarly to the skin of the human body it is feasible that ΔW_b and ΔW_s factors can be minimized to a similar level as gas pressurized suits, making MCP suits require significantly less work to be deformed. Minimizing ΔW_b and ΔW_s is challenging because the surface of the body undergoes a wide range of complex motions and deformations, which makes it difficult to model, engineer, and manufacture a MCP suit that maximizes mobility while maintaining an evenly distributed pressure [12].

Research on skin deformation and physiology dates back to the mid-1800s with one of the earliest publications by Karl Langer [13]. Langer studied the skin of cadavers and created diagrams that show the directions in which the skin deforms when punctured. The directions and lines are known as Langer Lines. Various lines and directions have been developed to determine optimal skin incision directions, which includes Pinkus main folding lines, Kraissl lines, and folding lines perpendicular to striae lines compiled by Lemperle *et al.* [14]. Space suit and bio-medical research has progressed our understanding of skin's deformation characteristics. The skin deformation at the knee joint was analyzed for the BioSuit™ [15–17] and for lower-limb prostheses [18]. Skin deformation at the ankle joint during flexion-extension and inversion-eversion was studied for developing active orthotics [19, 20]. Most recently, skin strain was mapped by the authors at the elbow joint using three dimensional digital image correlation (3D-DIC) with a spatial resolution of 1 mm^2 [12, 21]. These results showed that the magnitudes of

978-1-4673-7676-1/16/$31.00

deformation between subjects are similar, but the directional quantities can vary between subjects. It was also shown that LoNEs generally remained similar throughout elbow flexion for a given subject. The question remains of how skin deformation patterns change in joints with multiple degrees of freedom, such as the shoulder. If the deformation pattern in LoNEs can vary within a elbow joint, we hypothesize they could change in the shoulder joint.

The overall goal of this research is to understand the human body's natural skin strain field in order to drive the design of a MCP space suit that maximizes mobility by minimizing ΔW_b and ΔW_s. By measuring the skin strain field, materials and textile patterns can be developed to engineer a second skin-like garment. This research is also applicable to the biomedical field. Skin deformation data can be used in tissue engineering to design synthetic skin for plastic surgery. It can be also used to design exoskeletons, prostheses, and orthotics that interface with skin to maximize comfort and mobility. The specific aim of the research in this paper was to, first determine a method for analyzing complex joints, and second to understand how skin deformation is affected by different motions at the same joint for the same subject. For this specific study, the shoulder joint was measured during two isolated joint movements: shoulder flexion and abduction.

The contribution of this work is the methodology to measure skin strain at the shoulder joint using many stereoscopic camera pairs, a method to compare the directionality of skin strain fields, and data that shows how LoNEs vary during different motions of the shoulder joint. Results are presented and discussed in the context of realizing a mechanical counter pressure space suit for planetary exploration.

2. METHODS

Experimental Design

Skin deformation and strain at the shoulder joint of the human body was measured for one subject using three-dimensional digital image correlation. The subject performed shoulder flexion and shoulder abduction at joint angle increments of 15°. This experimental procedure was approved by the MIT Committee on the Use of Human Subjects (COUHES).

To perform 3D-DIC, a sufficiently random surface texture is required [22]. A speckle pattern was applied to the skin to create a unique texture. White Crayola Tempera was painted on with a brush. After the white paint dried, black Crayola Tempera paint was applied using a 3D printed speckle stamp manufactured out of ABS plastic on a Makerbot Replicator 2X. This application technique was developed previously by the authors [12]. These paints are non-toxic and washable. Figure 1 shows an example of the speckle pattern applied to the shoulder, which takes approximately 1 hour to apply.

Eight cameras (Basler acA2500-14gm, GigE, monochromatic, 5 megapixel, 16mm lenses) in four stereoscopic pairs were placed about the shoulder in order to view the joint throughout flexion, extension, and abduction. The cameras were synchronized using hardware triggering and were triggered at each joint angle increment. Three lights were attached to tripods to illuminate the surface of the body and reduce shadowing on the area of interest. This geometry presented significant challenges to continuously view throughout the motion without occlusion and without shadowing. This required the scene of the subject and camera placement to be modeled in computed-aided design (CAD) software. Figure

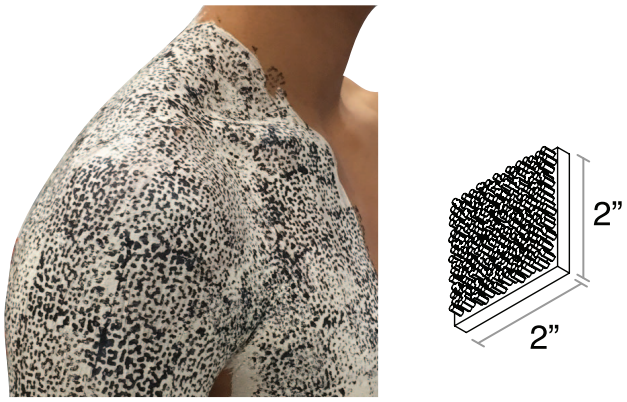

Figure 1. Speckle pattern applied to the shoulder with a white base and black speckles.

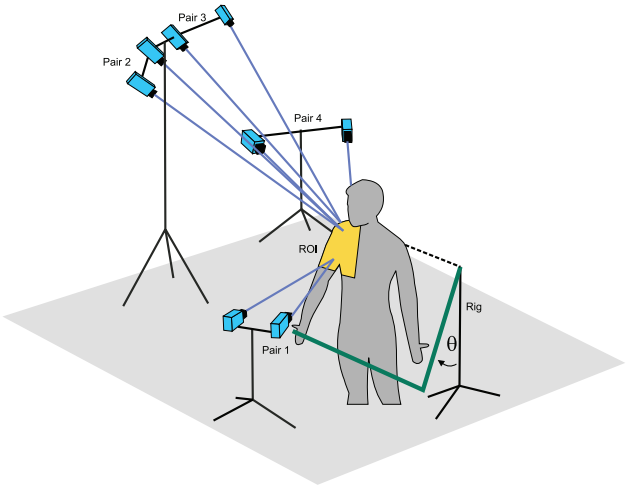

Figure 2. Experimental subject performing shoulder flexion guided by a mechanical rig. Eight cameras, in four stereoscopic pairs are setup to view the shoulder.

2 shows the camera and mechanical rig setup during shoulder flexion. The subject held the mechanical rig in order to guide the arm through the motion. The shoulder angle is denoted as θ and could be fixed and measured using a protractor. In the mechanical rig could be easily reconfigured to measure the abduction angle. The important aspect of the mechanical rig is to keep the rig's joint aligned with the shoulder rotation joint. This alignment is indicated in Figure 2 with a dashed line.

Prior to data collection, the camera system was calibrated using two sets of black and white dot pattern of a known size, which is shown in Figure 3. The calibration object was used to determine the optical properties of the cameras and the stereoscopic geometry. Calibration grid 1 could be seen by camera pairs 2, 3, and 4, while calibration grid 2 could be seen by camera pair 1. The relationship between the two sets of calibration dots is defined as a coordinate transformation with the rotation matrix, $\vec{R}$, and translation vector, $\vec{T}$. These parameters are determined by accurately measuring the calibration object with calipers. This coordinate transformation placed the stereoscopic camera pairs into the same coordinate system. Multiple calibration were not needed because the cameras remained fixed throughout the entire data collection period.

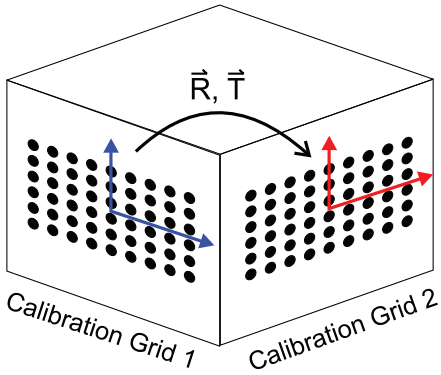

Figure 3. Calibration Object. Two grids used for stereoscopic calibration were mounted on a rectangular prism. The grids are related by a coordinate transformation defined by $\vec{R}$ and $\vec{T}$.

The subject gripped the mechanical rig with their right hand. The rig assured consistency of the arm positioning for all tests. The subject was positioned at increments of 15° joint angles using the mechanical rig starting at 0° shoulder flexion to 90° shoulder flexion and then 0° shoulder abduction to 90° shoulder abduction. Note that 0° shoulder flexion and abduction are the same position. The subject was instructed to keep their palm facing their side during flexion and abduction to avoid wrist rotation.

Data Analysis

Digital image correlation calculates the full surface strain field of the object. Ultimately this strain field can be used to calculate the LoNEs as originally described and shown by Arthur Iberall. This section briefly describes the data analysis process after obtaining strain data through 3D-DIC to LoNE calculations. More details on the data analysis process and calculations can be found in previous works by the author's [12].

The images were initially acquired using the MATLAB (Mathworks Inc., Natick, Massachusetts) image acquisition toolbox. The images were processed using VIC-3D, a commercial 3D-DIC software (Correlated Solutions Inc., Columbia, South Carolina). The commercial code calculates the displacement of pixel subsets in stereoscopic pairs of images. A subset size of 71 pixels was suggested by the software and used with a step size of 7 pixels. Assuming a working distance of approximately 1 meter, a horizontal angle of view of 20.2° for a 16mm lens, and a sensor with 2590 pixels wide this relates to a resolution of approximately 0.95 mm per data point. Green-Lagrange strain and Euler-Almansi strain was calculated with a Gaussian filter size of 15. In VIC-3D, this process can only be performed with stereoscopic camera pairs, therefore this process is repeated four times for each camera pair system. The data was exported to MATLAB to analyze strain directions and LoNE. In MATLAB, the data is transformed into one point cloud using the coordinate transformations of the calibration grid. The strain field from VIC-3D is calculated using a local two dimensional coordinate system and the out-of-plane strain components, E_{13}, E_{23}, E_{33}, are assumed to be zero, resulting in the 2D strain tensor for each mesh element:

$$\mathbf{E} = \begin{bmatrix} E_{11} & E_{12} \\ E_{12} & E_{22} \end{bmatrix}. \tag{2}$$

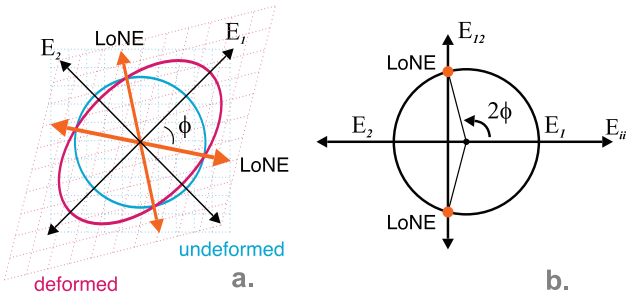

Figure 4. The Finite Strain Ellipse (a) and Mohr's Circle (b). The ellipse shows the Lines of Non-Extension (LoNE). There is no extensional strain along these lines, which is shown analytically in Mohr's circle.

The principal strain directions are calculated by an eigenvector analysis of the local strain field at each data point where $\vec{v}$ are the eigenvectors and λ are the eigenvalues of the strain tensor:

$$\mathbf{E}\vec{v} = \lambda\vec{v}. \tag{3}$$

The eigenvalues λ_1 and λ_2 are referred to as E_1 and E_2, respectively.

From the principal strain directions the directions of non-extension can be calculated by Equation 4 where ϕ is the angle from the principal strain direction. Note that directions of non-extension only exist if compression and tension are both present. Mathematically this is when E_1 and E_2 have opposite signs.

$$\phi = tan^{-1}\left(\sqrt{-\frac{E_1}{E_2}}\right) \tag{4}$$

We refer to the Finite Strain Ellipse and Mohr's Circle in Figure 4 to visualize this calculation. It is useful to frequently refer to this figure when working with the strain results.

The directions of principal strain and non-extension are now described as 2D vectors, however they need to be transformed into 3D. The commercial code computes the strain field with respect to a local 2D coordinate system on the surface of the object. The local coordinate system has the basis vectors $\mathbf{e_i'}$ and the global coordinate system has the basis vectors $\mathbf{e_i}$. The local coordinate system is defined with $\mathbf{e_3'}$ aligned along the surface normal vector, $\mathbf{e_1'}$ has no component along $\mathbf{e_2}$ and is orthogonal to the surface normal, and $\mathbf{e_2'}$ is the remaining orthogonal direction, $\mathbf{e_3'} \times \mathbf{e_1'}$. Using Equation 5 the vector fields can be rotated into the global reference frame. $\mathbf{X}'$ is local 2D vector field to be rotated, $\mathbf{X}$ is transformed the global 3D vector field, and $(\mathbf{e_j} \cdot \mathbf{e_i'})$ are the direction cosines. This is then expressed as $\mathbf{R}$, the rotation matrix.

$$\begin{aligned} \mathbf{X_i} &= (\mathbf{e_j} \cdot \mathbf{e_i'})\mathbf{X_j'} \\ \mathbf{e_j} \cdot \mathbf{e_i'} &= cos\theta_{ji} \\ \mathbf{X} &= \mathbf{R}\mathbf{X}' \end{aligned} \tag{5}$$

At this point in the analysis, there are four vector fields in the global frame: the first and second principal strain directions and the first and second lines of non-extension directions.

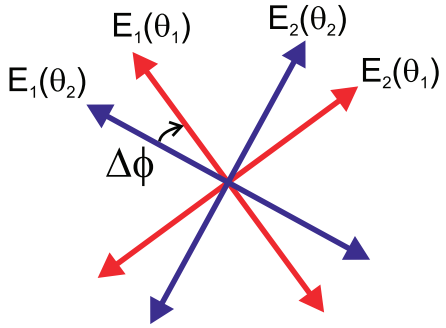

Figure 5. **$\Delta\phi$, the change in the angle between the principal strain components for two different motions described as θ_1 and θ_2.**

LoNEs are calculated from the directions of non-extension using a streamline procedure. The details for this procedure can be found in previous work on this topic [12, 21]. In summary, a LoNE is a contour that remains tangential to the non-extension direction. The LoNEs are calculated by treating the directions of non-extension as a vector field and integrating the vector field as streamlines tangential to the surface. In this implementation, the vector field was linearly interpolated and the Euler's method was used to integrate the vector field.

Human motion studies are typically subject to large variations between and even within subjects. However, there is one convenience in strain measurement data, which is the ability to express strain quantities in the original reference configuration. Here we use Green-Lagrange strain. Strain from one deformation can be directly compared on a point by point basis to the strain values in another deformation configuration because the data is mapped on the original geometry. This means that for each trial, shoulder flexion can be directly compared to shoulder abduction at every joint angle. We specifically examine the deviation of the directions of principal strain, $\Delta\phi$, using Equation 6, which is shown in Figure 5. Two different isolated movements are indicated by θ_1 and θ_2. The larger $\Delta\phi$ becomes, the less similar the principal strain directions are, which indicates the difference in the directional quantities of the strain field on a point by point basis.

$$\begin{aligned} \Delta\phi &= \phi(\theta_2) - \phi(\theta_1) \\ \phi(\theta_i) &= tan(E_{1y}(\theta_i)/E_{1x}(\theta_i))^{-1} \end{aligned} \tag{6}$$

3. Results

The results are divided into two sections. The first section, *Shoulder Flexion and Abduction*, looks in-depth at the strain data from shoulder flexion and abduction from one trial of one subject. This section also analyzes the differences in the strain field. The second section, *Repeated Trial*, gives insight into how the strain data can vary when the test is repeated.

Shoulder Flexion and Abduction

The strain results for one subject is shown in Figure 6. The data is shown from multiple views to account for the three-dimensional data. Shoulder flexion and abduction of 75° can be compared side by side. Shoulder abduction causes more deformation on the back near the under arm than flexion. However the strain magnitudes are generally in the same ranges. In addition to the strain magnitudes, the direction of the principal strain is shown by the black streak lines. From these lines it is visible that the direction of deformation changes between the two different movements.

Table 1. Deviation of principal strain direction

θ_1	θ_2	**Median**	**25%**	**75%**
Flexion 30°	Flexion 60°	5	0	12
Abduction 30°	Abduction 60°	-2	-7	2
Flexion 30°	Abduction 30°	31	29	57

From the strain data, the LoNEs can be calculated. Figure 7 shows the LoNEs calculated as streamlines for the shoulder joint during shoulder flexion at 75° and shoulder abduction at 75°. The red and blue indicate the first and second directions of non-extension and the light blue area indicates where there is a lack of directions of non-extension. Interestingly, this area moves shifts between abduction and flexion. In abduction, this shift results in less area for LoNEs to connect from the right shoulder blade to the right arm.

The deviation of the principal strain directions, $\Delta\phi$, was calculated between various movement states of deformation. Table 3 shows three comparisons that were made, which includes deviation within flexion, abduction, and between flexion and abduction. The distribution of angle deviation is not normal so the median, 25th and 75th percentile are reported. All units in the table are in degrees. The distribution of angle deviation is shown in Figure 8. For comparisons within the same type of isolated motion, the distribution tends to be centered near zero indicating that most of the strain is in the same direction. This feature is lost for the comparison between flexion and abduction. This results is consistent with the observations made in Figure 6. The same analysis for the directions of non-extension shows similar results.

Repeated Trial

The shoulder flexion and abduction experiment was repeated once. These results, although limited, are valuable for a preliminary understanding of measurement variability. Shoulder flexion at 30° of the subject is shown for trial 1 and for trial 2 with both principal strain magnitudes and directions. It can be seen that the magnitudes are similar, but vary and seem to be larger in trial 2 for the first principal strain magnitude.

4. Discussion and Conclusion

The strain field was measured using 3D-DIC and the LoNEs were calculated as continuous streamlines for the shoulder joint during flexion and abduction. The data collection required 4 stereoscopic pairs of camera (8 cameras total), a highly specific camera setup, and a new 3D calibration method using two calibration grids mounted to a rectangular prism. The principal strain directions were compared during shoulder flexion, shoulder abduction, and compared between shoulder flexion and abduction. This was made possible by analyzing the strain in the reference configuration, which removes the rigid body variability of the subject during motion.

Iberall stated, "Experimental study of the intrinsically limited motion at each joint verifies that this system of lines of non-

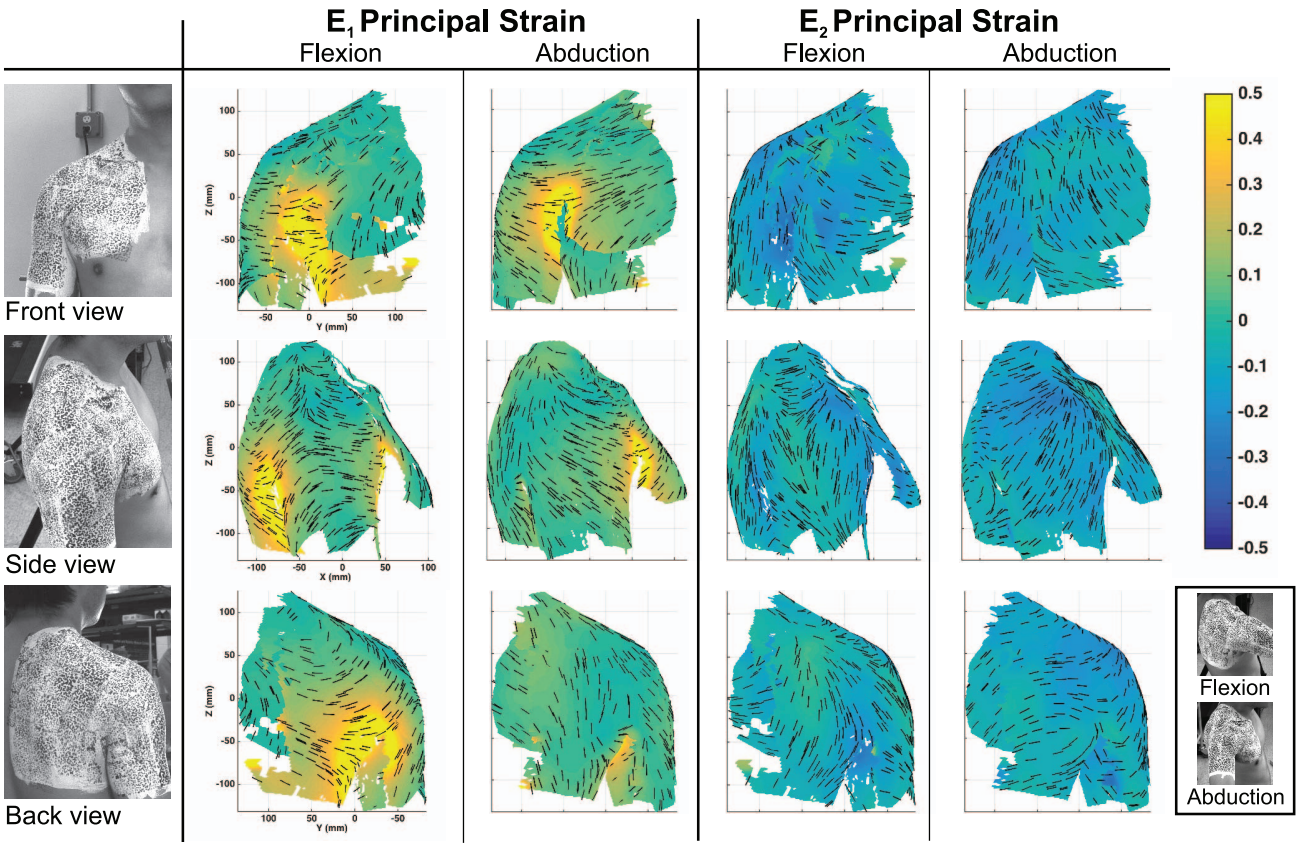

Figure 6. Strain results of one subject shown from different views. The first principal Green-Lagrange strain is shown in the first two columns for 75° shoulder flexion and 75° shoulder abduction. The second principal Green-Lagrange strain is shown in the last two columns for the same respective joint angles. All results are presented in the undeformed configuration. The black streaks indicate the direction of principal strain.

extension will be essentially the same for all deformations [2]." Although this was plausible for the elbow joint in the previous study by the authors [21], the data presented on the shoulder joint suggests that this may not be valid for more complicated joints. Considering Figure 6 and Figure 7 the strain field varies between two extreme motions such as shoulder flexion and abduction. It's conceivable that the strain fields would be more similar for more similar motions like shoulder flexion and extension. Caution should be taken when attempting to generalize LoNEs for one motion to other motions at the same joint.

Figure 9 showed that the strain magnitudes can change between repeated trials. It is most likely that this comes from the variability of the subject's positioning. Although a rig was used, the subject was kneeling and observably swaying during testing. Swaying can result in small image artifacts such as motion blur and a small movement forward or backwards could affect joint angle and therefore result in a change of strain in the body. For future trials, the experimental setup could be reconfigured so the subject is sitting or lying to minimize the variation in positioning.

One immediate limitation of this study is the inability to draw widespread conclusions from a single subject test. This preliminary study determined the optimal camera placement for shoulder tests as well as subject positioning. The sophisticated geometry of the shoulder led to challenges calibrating the system, changing shadowing conditions, maintaining the quality of the speckle pattern through extended testing periods, and maintaining the same area of interest throughout various isolated joint movements.

Now that a method has been developed to measure skin deformation for the shoulder more subjects will be tested. The experimental testing protocol will need to be sped up. The speckling method takes time to apply with a large surface area such as the shoulder. A larger stamp could be used or a new technique should be developed. The paint also requires time to dry to reduce glare. When the paint does dry it becomes flaky and can rub off. This is problematic for repeated trial testing unless the paint is reapplied. Another limitation is the difficulty to compare data between trials and between subjects. The anthropometric variability makes point by point comparisons nearly impossible, without using a deformable registration technique. In the future, the body should be segmented into feature areas, where the overall average areas for a region can be compared instead of a point by point comparison.

In addition to experimental test errors, DIC has systematic errors related to camera calibration, image matching, and 3D reconstruction error. Some error can be mitigated by camera setup, for instance, the stereoscopic angle is proportionally related to the in-plane displacement error and inversely proportional to the out-of-plane displacement error. Strain error in three dimensional DIC depends on various test conditions. Error in 3D DIC has been reported to be 0.01%-0.05% displacement error causing differences of 0.001 strain for controlled experiments [23]. The author's have performed

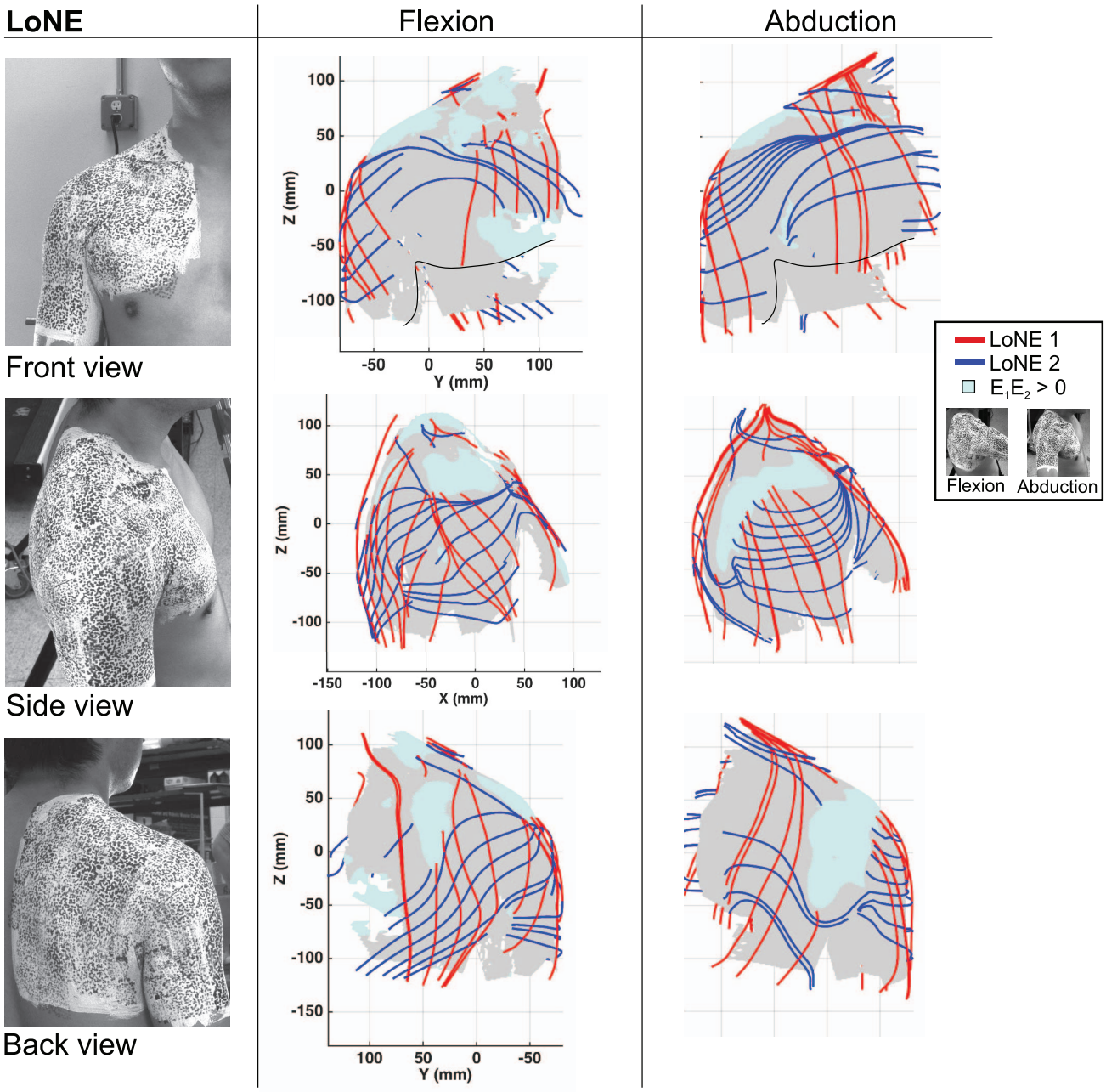

Figure 7. LoNEs shown from multiple views for 75° shoulder flexion and 75° shoulder abduction. The red and blue indicate the first and second direction of non-extension. The light blue region indicates areas that lack directions of non-extension.

validation tests with the equipment and methods more similar to conditions in the present study and have found the strain error to be 0.001-0.01 strain. The increase in strain error is from the complex 3D geometry of the body, large rigid body motions, large strains experienced by skin that can range from -0.5 to 0.5 strain and how the speckle pattern degrades over the course of the experiment. A more thorough analysis of the effect of strain error on LoNE can be found in previous work from the authors [12, p. 116]. DIC systems typically report reprojection error in pixels, but an analysis that carries this error through to strain error needs to be developed to understand the error on higher order analysis variables such as principal strain directions and non-extension directions.

Through this research, there is indication that the principal strain directions and LoNEs vary during shoulder flexion and abduction. It is conceivable that this finding may extend to other motions and other joints with multiple degrees of freedom, such as the hip. This variability needs to be taken into account when designing MCP space suits. A suit designed with shoulder flexion data may not be as mobile for shoulder abduction. By taking the information of both motions into account, it should be possible to design a garment that works well in both movement groups. Eventually, analysis of simple isolated joint movements will not be enough. Functional movements will need to be analyzed, with the hope that the strain fields of functional movements are the result of a linear combination of isolated joint motions. A future study

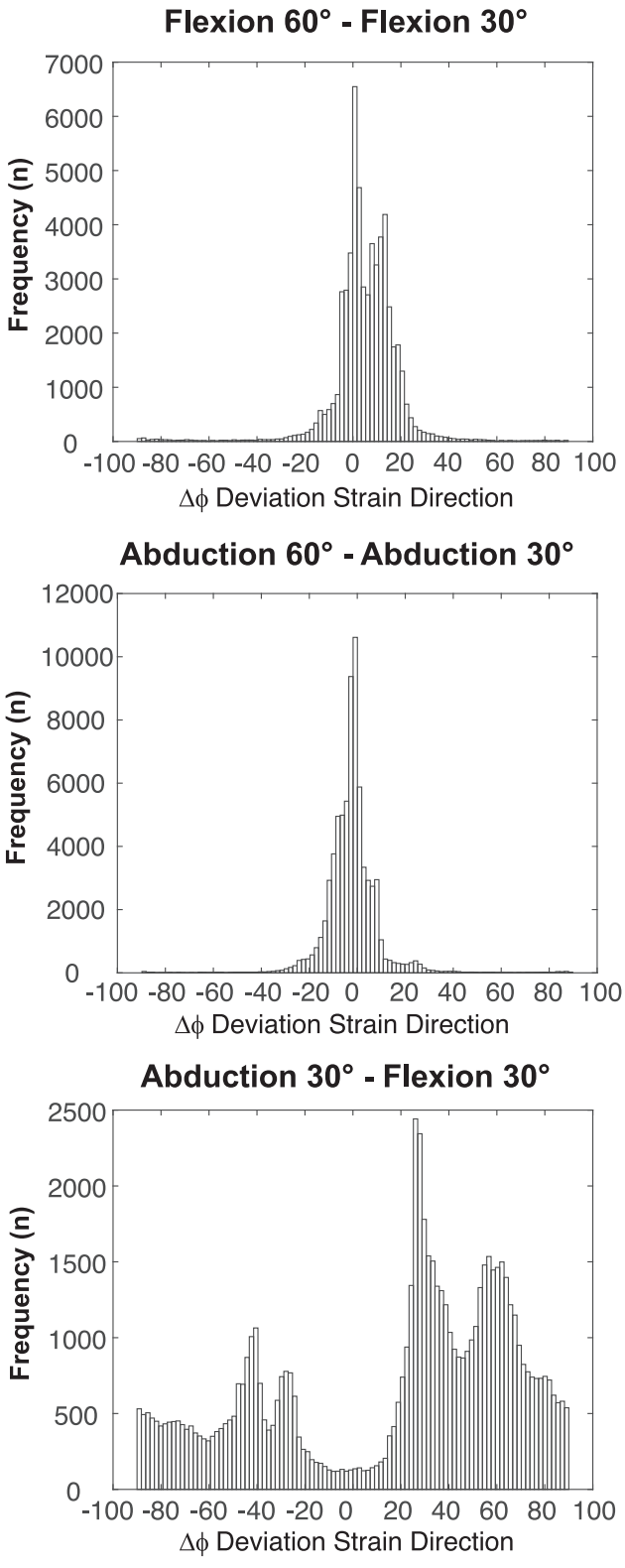

Figure 8. Distribution in the change in the principal strain direction between flexion at 30° and 60° (top), between abduction at 30° and 60° (middle), and flexion 30 ° and abduction 30° (bottom)

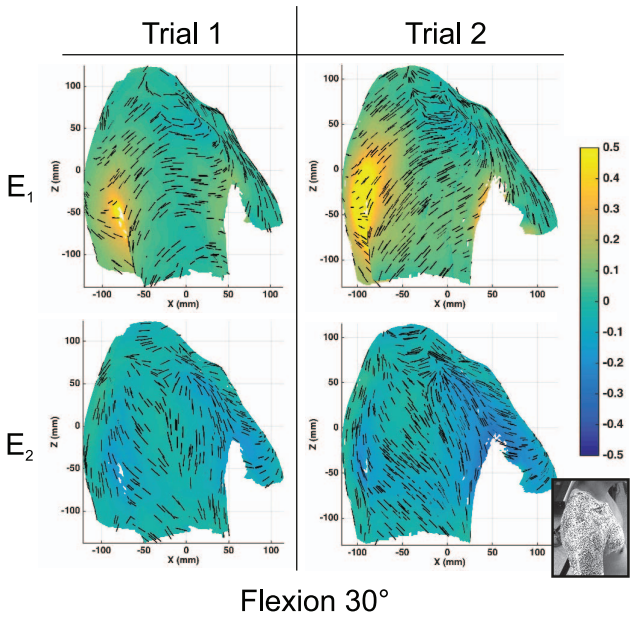

Figure 9. Shoulder flexion at 30° repeated twice. The first and second Green-Lagrange principal strains are shown with the direction indicated by black streak lines.

will be looking at shoulder movement with elbow movement to see how compound motions interact. Additionally more subjects need to be evaluated with a method for quantitatively comparing strain maps between subjects. An attempt will be made to develop a model of the strain field and LoNE map that is a function of human subject variables such as anthropometrics.

With an entire arm mapped and a strong understanding of the variability, the data will be used to design and develop a MCP arm sleeve that can be compared against gas-pressurized space suit arms. Engineering design is often a challenging iterative process, but through skin deformation analysis and the understanding of material deformation there are some key design principals to be considered. Some key mechanical principals of MCP suit design are as follows:

- MCP is most efficiently applied when stress is oriented in the direction of highest convex curvature *e.g.* stress provided in the circumferential direction of a limb provides MCP, whereas stress along the longitudinal direction does not.
- MCP attempts to mimic a state of hydrostatic pressure on the body, which means in some cases stress must not only exist in circumferential direction, but also in the longitudinal direction *e.g.* pressure needs to be applied around the circumference of the elbow or leg, but also at the end of the hand or foot along the direction of the limb to mimic a state of hydrostatic pressure.
- Material placed directly in contact with skin needs to be compatible with skin deformation. Large normal stresses applied by MCP will lead to excessive friction if there is material incompatibility. A mismatch in strain fields could result in chafing, friction blisters, or general discomfort.
- MCP garments should provide pretension in areas that develop compression throughout motions *e.g.* if no pretension exists in the material on top of the shoulder in the direction of the limb, shoulder abduction will lead to material buckling, which will result in local uneven areas of MCP that could cause bruising or edema.

In MCP space suit work there is often an emphasis on LoNE, but it is important to consider the entire strain field. In some aspects of suit design dealing with seams, sensors, wiring and cooling loops it will be beneficial to understand the directions of non-extension, but in areas that undergo large tensions and compression it will be necessary to know the magnitude of the body's deformation as well as the principal strain directions and the principal curvature directions, which is information provided by skin strain mapping. This information will allow the suit designer to align and orient suit material that efficiently provides mechanical counter pressure and does not inhibit mobility, which are often conflicting requirements. The human skin strain field map and LoNE geometry along with the understanding of it's variability between subjects will be used to develop the next version of the MIT BioSuit™.

ACKNOWLEDGMENTS

The authors thank the Office of Naval Research and the MIT Portugal Program for funding this project, Midé Technologies, Professor Tomasz Wierzbicki and Kai Wang at the MIT Impact and Crashworthiness Laboratory, and Professor Raul Radovitzky, Dr. Aurélie Jean and Dr. Martin Hautefeuille at the MIT Institue of Soldier Nanotechnology. Special and exceptional thanks goes to undergraduate researcher, Hamilton Eng, for designing the experimental setup.

REFERENCES

[1] L. D. Kozloski, *U.S. space gear: outfitting the astronaut*. Washington: Smithsonian Institution Press, 1994.

[2] S. Iberall, "Experimental design of a mobile pressure suit," *Journal of Basic Engineering*, vol. 92, no. 2, pp. 251–364, 1970.

[3] J. F. Annis and P. Webb, "Development of a space activity suit," NASA, Report, 1971.

[4] B. Pitts, J. Brensinger, C. andSaleh, C. Carr, P. Schmidt, and D. Newman, "Astronaut bio-suit for exploration class missions," Massachusetts Institute of Technology, Report, 2001.

[5] D. J. Newman, M. Canina, and G. L. Trotti, "Revolutionary design for astronaut exploration - beyone the bio-suit system," pp. 975–986, February 2007.

[6] K. Tanaka, P. Danaher, P. Webb, and A. R. Hargens, "Mobility of the elastic counterpressure space suit glove," *Aviation Space Environmental Medicine*, vol. 10, no. 0095-6562 (Print), pp. 890–3, 2009.

[7] W. M. Clapp, *Design and testing of an advanced spacesuit glove*, ser. SSL: # 14-83. Cambridge, MA : Space Systems Laboratory, Dept. of Aeronautics and Astronautics, Massachusetts Institute Technology, 1983., 1983.

[8] J. M. A. Waldie, K. Tanaka, D. Tourbier, P. Webb, C. W. Jarvis, and A. R. Hargens, "Compression under a mechanical counter pressure space suit glove," *Journal Of Gravitational Physiology: A Journal Of The International Society For Gravitational Physiology*, vol. 9, no. 2, pp. 93–97, 2002.

[9] G. L. Harris, *The origins and technology of the advanced extravehicular space suit.* San Diego, CA: American Astronautical Society, 2001.

[10] P. B. Schmidt, "An investigation of space suit mobility with applications to eva operations." Thesis, Massachusetts Institute of Technology, 2001.

[11] C. E. Carr and D. J. Newman, "Space suit bioenergetics: Framework and analysis of unsuited and suited activity," *Aviation Space and Environmental Medicine*, vol. 78, no. 11, pp. 1013 – 1022, 2007.

[12] E. W. Obropta, "On the deformation of human skin for mechanical counter pressure space suit development," Thesis, Massachusetts Institute of Technology, 2015.

[13] K. Langer, "On the anatomy and physiology of the skin," *British Journal of Plastic Surgery*, vol. 17, no. 31, pp. 93–106, 1861.

[14] G. Lemperle, M. Tenenhaus, D. Knapp, and S. M. Lemperle, "The direction of optimal skin incisions derived from striae distensae." *Plastic And Reconstructive Surgery*, vol. 134, no. 6, pp. 1424 – 1434, 2014.

[15] K. Bethke, D. J. Newman, and R. Radovitzky, "Creating a skin strain field map with application to advanced locomotion spacesuit design," 2005.

[16] N. Wolfrum, N. D.J., and K. Bethke, "An automatic procedure to map the skin strain field with application to advanced locomotion space suit design," Cleveland, OH, July 2006.

[17] A. M. Wessendorf and D. J. Newman, "Dynamic understanding of human-skin movement and strain-field analysis," *Ieee Transactions on Biomedical Engineering*, vol. 59, no. 12, pp. 3432–3438, 2012, wessendorf, Ashley M. Newman, Dava J.

[18] A. T. Marecki, "Skin strain analysis software for the study of human skin deformation," Thesis, Massachusetts Institute of Technology, 2012.

[19] A. R. Domingues, J. Martins, M. Silva, and D. Newman, "Analysis of the human ankle impedance for the design of active soft orthosis," August 2013.

[20] S. P. Marreiros, A. R. Domingues, J. Martins, M. T. Silva, and D. J. Newman, "Computational calculation and representation of the lines of non-extension of the ankle-foot complex," June 2013.

[21] E. Obropta and N. D.J., "A comparison of human skin strain fields of the elbow joint for mechanical counter pressure space suit development," Bik Sky, Montana, March 2015.

[22] H. W. Schreier, J.-J. Orteu, and M. A. Sutton, *Image Correlation for Shape, Motion and Deformation Measurements : Basic Concepts, Theory and Applications*. New York, N.Y.: Springer, 2009, accession Number: 277000. Publication Type: eBook. Language: English.

[23] T. Becker, K. Splitthof, T. Siebert, and P. Kletting, "Error estimations of 3d digital image correlation measurements," Dantec Dynamics, Report, 2006.

BIOGRAPHY

Edward Obropta *received the Bachelor of Science degree in 2013, the Master of Science degree in 2015 in aerospace engineering, and is currently pursuing a doctoral degree, from the Massachusetts Institute of Technology (MIT). His research interests include bioastronautics, space suit design, solid mechanics, active materials, and sports technology.*

Dr. Dava Newman *is currently on leave from MIT serving as the NASA Deputy Administrator. Dr. Newman was the Apollo Program Professor of Astronautics at the Massachusetts Institute of Technology (MIT) and affiliate faculty in the Harvard-MIT Health Sciences and Technology Program. Her expertise is in multidisciplinary research that encompasses aerospace biomedical engineering. Dr. Newman's research studies were carried out through space flight experiments, ground-based simulations, and mathematical modeling. Her past research efforts included: advanced space suit design, dynamics and control of astronaut motion, mission analysis, and engineering systems design and policy analysis. She also had ongoing efforts in assistive technologies to augment human locomotion here on Earth. Dr. Newman is the author of Interactive Aerospace Engineering and Design, an introductory engineering textbook published by McGraw-Hill, Inc. in 2002. She has published more than 250 papers in journals and refereed conferences.*